Journal of Sound and Vibration 329 (2010) 1081–1088

Contents lists available at ScienceDirect

Journal of Sound and Vibration

journal homepage: www.elsevier.com/locate/jsvi

Dynamics of microscale pipes containing internal fluid flow: Damping, frequency shift, and stability

Stephanie Rinaldi, Sairam Prabhakar, Srikar Vengallatore *, Michael P. Païdoussis

Department of Mechanical Engineering, McGill University, 817 Sherbrooke Street West, Montreal, QC, Canada H3A 2K6

ARTICLE INFO

Article history:
Received 16 March 2009
Received in revised form
19 August 2009
Accepted 17 October 2009
Handling Editor: A.V. Metrikine
Available online 17 November 2009

ABSTRACT

This paper initiates the theoretical analysis of microscale resonators containing internal flow, modelled here as microfabricated pipes conveying fluid, and investigates the effects of flow velocity on damping, stability, and frequency shift. The analysis is conducted within the context of classical continuum mechanics, and the effects of structural dissipation (including thermoelastic damping in hollow beams), boundary conditions, geometry, and flow velocity on vibrations are discussed. A scaling analysis suggests that slender elastomeric micropipes are susceptible to instability by divergence (buckling) and flutter at relatively low flow velocities of ~10 m/s.

1. Introduction

Miniaturized beam and plate resonators are the core components of microelectromechanical systems (MEMS) used for applications ranging from sensing and communications to energy harvesting and fundamental studies of quantum mechanical systems [1]. Across these disparate applications, the design of high-performance microresonators is dominated by three basic requirements. The first is to attain high values for the natural frequency of vibration (10 kHz to 1 GHz) to enable sensing at high rates and match the frequencies of the signals of interest. The second is to reduce the damping factor to low values between 10^{-6} and 10^{-4} (or, equivalently, attain a high mechanical quality factor, Q, between 10 000 and a million), so as to enhance sensitivity and frequency selectivity. The third is to ensure the stability of vibrations and minimize any drift in the operating frequency due to nonlinear effects and environmental coupling [2].

The design parameters that can be tailored to meet these requirements are the material properties, size, geometry, boundary conditions, and modal properties. The design of microresonators used for sensing was initially dominated by structures with solid rectangular cross-sections, partly due to the constraints imposed by microfabrication technologies; however, subsequent generations have grown increasingly sophisticated in terms of their structural design and mode shapes. In this paper, we focus on a class of microresonators that may be characterized as *micropipes containing internal fluid flow* [3–10].

Flow-containing micropipes enable resonant sensing in a manner that combines a high Q (in excess of 10 000) with the ability to interrogate a fluidic specimen [3–8]. Sensing is achieved by operating the device within an evacuated chamber and detecting small changes in the natural frequency (of the order of one part in a million). Quantifying the effects of flow on damping and frequency shift is essential for the design and operation of such sensors. Another device, aptly described as a "micromachined fountain pen", is used for local surface patterning and direct-write lithography [9,10]. These cantilevered

* Corresponding author. Tel.: +1 514 398 2174.
E-mail address: srikar.vengallatore@mcgill.ca (S. Vengallatore).

0022-460X/$ - see front matter © 2009 Elsevier Ltd. All rights reserved.
doi:10.1016/j.jsv.2009.10.025

micropipes are connected to a fluidic reservoir at the clamped end, and eject fluid from the free end; hence, preventing any flow-induced instability is a key requirement for successful operation.

The effects of internal fluid flow on the dynamics and stability of macroscale structures, with dimensions ranging from a few centimeters to tens of meters, have been extensively studied for over 60 years (see, for example, [11]). Depending upon the details of the fluid-structure interactions (FSI), increasing the flow can lead to a shift of the natural frequency, change of the damping factor, and both static and dynamic instabilities in the form of buckling and flutter. More recently, several studies of FSI in nanometer-scale structures have been published in connection with flow through carbon nanotubes (see, for example, [12–14]). However, the intermediate range of micrometer-scale structures, which is of interest for MEMS, remains largely unexplored. This motivates the work presented in this paper. We consider the dynamics of the relatively simple, but technologically relevant, case of straight micromachined pipes containing internal fluid flow, and present results for the effects of scale, materials, and flow velocity on damping, frequency shift, and stability.

2. Analysis using classical continuum mechanics

The structures under consideration are modelled as straight and slender micromachined pipes of length L between supports, flexural rigidity EI, and mass per unit length m. The cross-section of the pipe is symmetric, either circular or rectangular, and may contain one or a set of parallel internal channels, as illustrated in Fig. 1. In all cases, the smallest structural dimension exceeds 1 μm; thus, for the circular pipe of Fig. 1(a), $1\,\mu m < D_i < 100\,\mu m$, $0.1 < (D_i/D_o) < 0.5$ and $(L/D_o) > 10$. The axisymmetric internal flow in the micromachined pipe is due to a viscous, incompressible, single-phase fluid of mass per unit length M flowing with velocity U. The cross-section contains millions of atoms for the solids and fluids of interest in these flow-containing micropipes, which suggests that the use of continuum theories is appropriate for analyzing the effects of flow on dynamics.

Over the past two decades, the constitutive relationships and laws of classical continuum mechanics (including Hooke's law for elasticity, generalized Hooke's law for thermoelasticity, Fourier's law for heat conduction, Navier–Stokes equation for fluid flow, and Euler–Bernoulli theory for slender elastic structures) have been extensively used to analyze the static and dynamic behavior of microscale structures, and to analyze flow through micrometer-scale channels. These studies were motivated by the need to design the components of MEMS for numerous applications, as documented in several textbooks and monographs (see, for example, [15–18]), and reflect a growing consensus on the utility and validity of classical continuum theories at micrometer length scales.

Mathematical models based on continuum mechanics contain structural geometry and material properties as parameters, and the effects of scale can be studied by analyzing these models. Many properties—including elastic modulus, density, Poisson's ratio, coefficient of linear expansion, and specific heat—exhibit essentially the same values for both macroscale and microscale specimens of common engineering materials [15,19]. In contrast, the yield strength, fracture strength, and internal friction can be strong functions of size, processing methods, and microstructure; measurements on microscale specimens are usually necessary to obtain their values [20]. Fortunately, these properties are not relevant for the problems under consideration here.

For the sake of completeness, we note that the validity of classical continuum theories must be re-examined if structures are further miniaturized down to nanometer dimensions, and operated in extreme environments. Deviations from classical Navier–Stokes behavior are expected when the channel dimensions are comparable to the diameter of the molecules comprising the fluid [21,22]. Similarly, Fourier's law may not be accurate for heat conduction across nanoscale

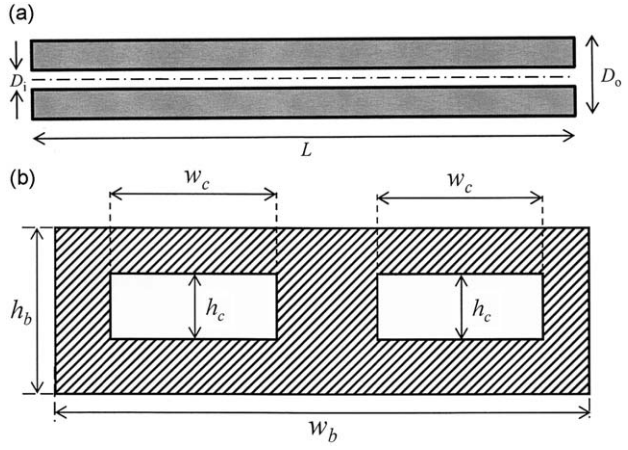

Fig. 1. (a) Illustration of a straight pipe of length L containing internal channels of circular cross-section with outer diameter D_o and inner diameter D_i. (b) Illustration of the doubly symmetric rectangular cross-section of a pipe containing a pair of parallel channels of width w_c and height h_c. The width and thickness of the pipe are denoted w_b and h_b, respectively.

structures when the mean free paths of the quanta of heat transport are comparable to structural dimensions [23]. Other deviations from classical behavior are expected if the temperature is reduced to extremely low values of the order of 1 K. Indeed, accessing the quantum states of micro- and nanomechanical resonators at cryogenic temperatures is a topic of intense current research [24].

Taken together, these arguments suggest that classical continuum theories can be used with confidence to analyze the dynamics of microscale pipes containing internal flow. Therefore, the vast and rich literature on FSI in macroscale structures can be harnessed to study the effects of miniaturization on dynamics. A natural starting point for our analysis is the well-established equation of motion for a straight pipe conveying flow.

2.1. Equation of motion

The simplest linearized equation for the free, damped flexural vibrations of a flow-containing pipe is [11,25,26]

$$EI\left[1+\left(\alpha+\frac{\mu}{\Omega}\right)\frac{\partial}{\partial t}\right]\frac{\partial^4 w}{\partial x^4}+MU^2\frac{\partial^2 w}{\partial x^2}+2MU\frac{\partial^2 w}{\partial x\,\partial t}+c\frac{\partial w}{\partial t}+(M+m)\frac{\partial^2 w}{\partial t^2}=0, \tag{1}$$

where $x\in[0,L]$ is the axial coordinate, t is time, and $w(x,t)$ is the lateral deflection. This equation ignores the effects of gravity, but includes the effects of dissipation in the fluid and in the material of the pipe, with the latter modelled as a combination of hysteretic and viscoelastic damping. Here, μ is the dimensionless hysteretic damping coefficient, Ω is the circular frequency, α is the viscoelastic damping coefficient modelled using a two-parameter Kelvin–Voigt model, and c denotes the viscous damping coefficient due to the fluid (air) surrounding the pipe. The equation for undamped free vibrations is recovered by setting α=0, μ=0 and c=0 in Eq. (1).

Eq. (1) is valid for the flow of a single-phase fluid that completely fills the channel, and the flow is modelled as a plug-flow, which is quite appropriate for fully developed turbulent flow.[1] The fluid itself is assumed to be viscous; however, viscosity-related terms do not appear explicitly in the equation of motion because the viscous traction on the pipe and viscous pressure-loss forces exactly cancel out in the linear limit. The hysteretic damping, μ, is typically used to analyze the response to a harmonic excitation, but can also be used to obtain useful approximations of the free response for lightly damped systems—i.e., provided that the damping ratio, ζ, is small compared to unity [11].

For convenience, Eq. (1) can be expressed in non-dimensional form as

$$\left(\overline{\alpha}+\frac{\mu}{\omega}\right)\dot{\eta}''''+\eta''''+u^2\eta''+2\sqrt{\beta}u\dot{\eta}'+\sigma\dot{\eta}+\ddot{\eta}=0, \tag{2}$$

where

$$\xi=\frac{x}{L},\quad \eta=\frac{w}{L},\quad \tau=\sqrt{\frac{EI}{M+m}}\frac{t}{L^2},\quad u=\sqrt{\frac{M}{EI}}LU,\quad \beta=\frac{M}{M+m},\quad \omega=\sqrt{\frac{M+m}{EI}}\Omega L^2, \tag{3}$$

and the spatial and temporal derivatives are given by $\eta'=(\partial\eta/\partial\xi)$ and $\dot{\eta}=(\partial\eta/\partial\tau)$. The dimensionless viscoelastic damping, $\overline{\alpha}$, and the dimensionless viscous damping, σ, are defined as

$$\overline{\alpha}=\sqrt{\frac{EI}{M+m}}\frac{\alpha}{L^2},\quad \sigma=\frac{cL^2}{\sqrt{EI(M+m)}}. \tag{4}$$

All the details of the cross-sectional shape are captured by the dimensionless mass fraction, β, in this one-dimensional model.

3. Scaling analysis of stability

The stability of systems governed by Eq. (2) has been extensively analyzed, and the principal results may be summarized in terms of the non-dimensional critical flow velocity, u_c [11]. The first instability occurs by divergence for beams with both ends supported, and by single degree-of-freedom flutter for cantilevered beams. The dimensionless critical velocities for pinned–pinned and clamped–clamped beams are $u_c=\pi$ and 2π, respectively, independent of dissipation or β. In contrast, $u_c\simeq 5$ or larger for cantilevers, and this value depends on the type of damping and β [11].

The corresponding dimensional values of the critical flow velocities, U_c, follow directly from Eq. (3). Thus, for the beam with circular cross-section shown in Fig. 1(a), we obtain

$$\frac{U_c}{u_c}=\sqrt{\frac{EI}{M}}\frac{1}{L}=\frac{1}{4L}\sqrt{\frac{E(D_o^4-D_i^4)}{\rho_f D_i^2}}=\sqrt{\frac{E}{\rho_f}}\frac{\sqrt{1-\lambda_1^4}}{4\lambda_1\lambda_2}. \tag{5}$$

Here ρ_f is the fluid density, $\lambda_1=(D_i/D_o)$ is the cross-sectional aspect ratio, and $\lambda_2=(L/D_o)$ is the slenderness ratio. Using Eq. (5), the critical flow velocity was plotted as a function of these two aspect ratios for different classes of engineering

[1] If, however, the flow is laminar and modelled as a Poiseuille flow, the definition of M and U in MU^2 and MU would strictly need to be refined; but, in accordance with Benjamin's arguments [27], the effect on the dynamics is expected to be small.

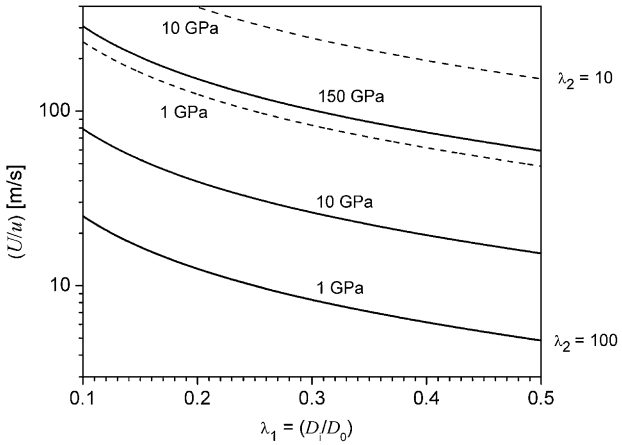

Fig. 2. The effect of material properties and beam aspect ratios on the critical velocities for instability. The discontinuous and solid lines denote beams with $\lambda_2 = (L/D_o) = 10$ and λ_2=100, respectively. The elastic modulus corresponding to each curve is indicated on the graph.

materials: elastomers (1 GPa$<E<$10 GPa), metals (70 GPa$<E<$200 GPa), and ceramics (100 GPa$<E<$450 GPa). In all cases, the fluid within the pipe is water (ρ_f=10^3 kg/m^3). Fig. 2 shows that, for beams with a low slenderness ratio of $(L/D_o) = 10$, the critical flow velocities exceed several hundred meters per second for all materials. At such high flow velocities, other factors, including the possibility of cavitation [28], must be included in the analysis. However, for slender elastomeric pipes with $(L/D_o) = 100$, the critical velocities reduce to $\sim$10 m/s, which implies that instability during operation must be factored into the design of such devices. This analysis can readily be extended to analyze the effects of different materials and cross-sectional shapes on stability.

4. Analysis of damping and frequency shifts

The effects of miniaturization on damping are not susceptible to simple scaling analyses because of the inherent complexity and variety associated with dissipative phenomena, and because many important aspects of damping remain unexplored at all length scales. Two such issues of relevance to MEMS are: (i) the relative importance of different damping mechanisms, and (ii) the quantification of the ultimate limits on damping established by a combination of thermoelastic damping (TED) and flow-induced damping, thereby establishing the absolute upper limit on the performance of resonant microsensors. These open questions can be addressed by solving Eq. (2), subject to appropriate boundary conditions, to obtain the complex eigenfrequencies, ω; the real part is the dimensionless oscillation frequency, and the ratio of the imaginary and real parts is the damping ratio of the system, $\zeta = \mathrm{Im}(\omega)/\mathrm{Re}(\omega)$.

Using the Galerkin method, the complex eigenfrequencies were obtained for beams of two different materials (single-crystal silicon and a representative elastomer) with rectangular and circular cross-sections. For each case, five different damping models were studied: (i) no damping ($\sigma = 0$, $\overline{\alpha} = 0$, $\mu = 0$), (ii) viscous damping ($\sigma \neq 0$, $\overline{\alpha} = 0$, $\mu = 0$), (iii) viscoelastic damping ($\sigma = 0$, $\overline{\alpha} \neq 0$, $\mu = 0$) (iv) hysteretic damping ($\sigma = 0$, $\overline{\alpha} = 0$, $\mu \neq 0$) and (v) a combination of all types of damping ($\sigma \neq 0$, $\overline{\alpha} \neq 0$, $\mu \neq 0$). To begin with, the dimensionless viscous damping constant was set equal to a realistic value, i.e. σ=0.01. Thereafter, the dimensionless viscoelastic, $\overline{\alpha}$, and hysteretic, μ, damping coefficients were chosen to let the value of the first-mode damping factor, ζ_1, at zero flow velocity, i.e. u=0, be identical to the first-mode damping factor, ζ_1, for the case of σ=0.01 This method of determining the individual damping factors was utilized in an effort to demonstrate the relative importance of each type of damping on the dynamics of this system.

Typical results are presented in Table 1 for pinned–pinned and cantilevered elastomeric pipes of circular cross-section with β=0.14. A comparison of the values of the dimensionless complex eigenfrequencies and damping factors at u=2.00 for the two lowest modes, along with the values of the critical flow velocities, u_c, shows that the viscoelastic and hysteretic damping models lead to identical results. The critical flow velocity for flutter in the second mode of the cantilevered pipe ranges from 5.06 to 5.15, depending on the type of damping.

Subsequently, the hysteretic damping was modelled as thermoelastic damping ($\mu = \mu_{\mathrm{TED}}$, $\sigma = 0$, $\overline{\alpha} = 0$). This mechanism arises as a consequence of the coupling between strain and temperature fields in flexural-mode resonators, and establishes the absolute lower bound on material damping [29–32]. Moreover, some microscale resonators (including the practically important case of single-crystal silicon beams) can be designed to operate at the thermoelastic limit. Recently, expressions for the frequency dependence of μ_{TED} in hollow micropipes have been presented in the form of an infinite series [33]. These expressions do not contain any free parameters, and were obtained by solving the thermoelastic heat conduction equation with the assumption of one-way coupling—that is, the stress field generates a temperature field

Table 1
Some quantitative results at u=2.00 and $u=u_c$ for an elastomer pipe with β=0.14.

	Cantilevered system				
	No damping	**Viscous damping σ=0.01**	**Viscoelastic damping $\overline{\alpha}=8.09\times10^{-4}$**	**Hysteretic damping $\mu=2.84\times10^{-3}$**	**Combination of $\sigma,\overline{\alpha}$ and μ**
First mode ω at u=2.00	3.6883+1.5994i (ζ=0.4336)	3.6862+1.6043i (ζ=0.4352)	3.6865+1.6044i (ζ=0.4352)	3.6865+1.6044i (ζ=0.4352)	3.6826+1.6143i (ζ=0.4384)
Second mode ω at u=2.00	20.8349+1.4326i (ζ=0.0688)	20.8345+1.4377i (ζ=0.0690)	20.8189+1.6288i (ζ=0.0782)	20.8189+1.6288i (ζ=0.0782)	20.8007+1.8301i (ζ=0.0880)
u_c	5.06 (2nd mode flutter)	5.07 (2nd mode flutter)	5.11 (2nd mode flutter)	5.11 (2nd mode flutter)	5.15 (2nd mode flutter)
Second mode ω_c at $u=u_c$	14.0333–0.0000i (ζ=0)	14.0153–0.0000i (ζ=0)	13.8775–0.0000i (ζ=0)	13.8775–0.0000i (ζ=0)	13.7390–0.0000i (ζ=0)
	Pinned–pinned system				
	No damping	**Viscous damping σ=0.01**	**Viscoelastic damping $\overline{\alpha}=1.03\times10^{-4}$**	**Hysteretic damping $\mu=1.01\times10^{-3}$**	**Combination of $\sigma,\overline{\alpha}$ and μ**
First mode ω at u=2.00	7.5654+0.0000i (ζ=0)	7.5654+0.0049i (ζ=0.0007)	7.5654+0.0050i (ζ=0.0007)	7.5654+0.0050i (ζ=0.0007)	7.5654+0.0149i (ζ=0.0020)
Second mode ω at u=2.00	37.4869+0.0000i (ζ=0)	37.4869+0.0050i (ζ=0.0001)	37.4868+0.0800i (ζ=0.0021)	37.4868+0.0800i (ζ=0.0021)	37.4865+0.1650i (ζ=0.0044)
u_c	3.15 (1st mode buckling)	3.15 (1st mode buckling)	3.15 (1st mode buckling)	3.15 (1st mode buckling)	3.15 (1st mode buckling)

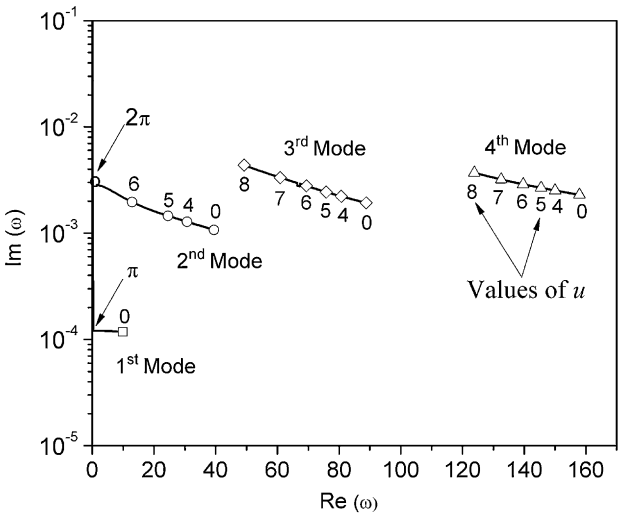

Fig. 3. Dimensionless complex frequency graph (Argand diagram) as a function of the dimensionless flow velocity, u, for a thermoelastically damped, pinned–pinned, single crystal silicon micropipe with β=0.1. The first two modes become unstable by divergence at critical flow velocities of π and 2π, respectively; for $u>\pi$, the first-mode locus lies on the Im(ω)-axis, and so does the second-mode locus just beyond $u=2\pi$.

during vibration, but is itself unaffected by the resulting changes in temperature; this is valid because the temperature changes under consideration are always small (typically, <0.1 percent for a beam originally at 300 K). For the same reason, the fluidic field is also unaffected by any changes in temperature due to the thermoelastic effect; thus, the effects of TED can be appropriately modelled by setting $\mu=\mu_{\mathrm{TED}}$ in Eq. (2).

Typical results are presented in the form of Argand diagrams, with axes corresponding to the imaginary and real parts of the dimensionless complex eigenfrequency, for the representative cases of pinned–pinned and cantilevered single-crystal silicon micropipes containing a pair of parallel internal channels, as shown in Fig. 1(b), with h_b=7 μm, w_b=33 μm, h_c=3 μm, and w_c=8 μm. Simple closed-form expressions for TED in this structure, along with material properties for silicon at 300 K, were obtained from Ref. [33].

The Argand diagram for the pinned–pinned beam in Fig. 3 is plotted on a semi-log graph because of the relatively low level of damping in this system. At u=0, the dissipation is entirely due to thermoelastic damping. As u is gradually increased, Im(ω) increases slightly, but Re(ω) diminishes at a faster rate. Therefore, as the flow velocity increases, the

frequencies of oscillation are diminished and the damping factors are increased. This continues until a critical value of u at which the system becomes unstable by divergence. As expected [25], $u_c=\pi$ for the first mode, and $u_c=2\pi$ for the second mode. Beyond the point of divergence, the behavior of the system must be analyzed using nonlinear theory [11]. The third and fourth modes are stable over the range of non-dimensional flow velocities investigated in this study.

Fig. 3 shows that $\mathrm{Re}(\omega)\to 0$ for u near π for the first mode. Hence, the hysteretic component of the damping model, as well as the precise values of $\mathrm{Im}(\omega)$, become questionable in this range of u. However, the main interest lies in the predicted values of $\mathrm{Im}(\omega)$ and ζ in the practically important range $0\le u<2$, as well as in obtaining u_c. Calculations with the hysteretic damping excised, and the viscoelastic component augmented so as to give the same total damping at $u=0$, yield an Argand diagram not perceptibly different from that in Fig. 3. This observation is entirely consistent with the results presented in the third ($\overline{\alpha}\neq 0$) and fourth ($\mu\neq 0$) columns of Table 1 for the elastomeric pipe.

The Argand diagram for the cantilevered system is shown in Fig. 4. As u is gradually increased, $\mathrm{Im}(\omega)$ increases at a much faster rate compared to the pinned–pinned beam, signifying that the system is subject to considerable flow-induced

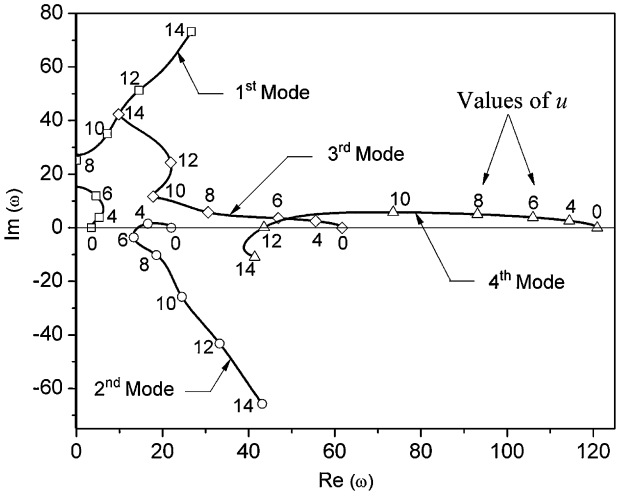

Fig. 4. Dimensionless complex frequency graph (Argand diagram) as a function of the dimensionless flow velocity, u, for a thermoelastically damped, cantilevered, single crystal silicon micropipe with β=0.1. In the scale of this figure, $\mathrm{Im}(\omega)$ at u=0 appears to be zero, though in fact it is not; e.g. $\mathrm{Im}(\omega)$ attains values of 1.5×10^{-5} and 5×10^{-4} for the first and second modes, respectively, at u=0.

Table 2
Some quantitative results at u=2.00 and $u=u_c$ for a silicon micropipe with β=0.1.

	No damping	**Viscous damping σ=0.01**	**Thermoelastic damping, μ_{TED} [33]**	**Viscous damping and TED σ, μ_{TED}**
Cantilevered system				
First mode ω at u=2.00	3.7882+1.3772i (ζ=0.3635)	3.7864+1.3821i (ζ=0.3650)	3.7882+1.3772i (ζ=0.3636)	3.7864+1.3821i (ζ=0.3650)
Second mode ω at u=2.00	20.8191+1.2216i (ζ=0.0587)	20.8188+1.2267i (ζ=0.0589)	20.8190+1.2221i (ζ=0.0587)	20.8187+1.2272i (ζ=0.0589)
u_c	4.78 (2nd mode flutter)	4.79 (2nd mode flutter)	4.78 (2nd mode flutter)	4.79 (2nd mode flutter)
Second mode ω_c at $u=u_c$	14.2182–0.0000i (ζ=0)	14.1932–0.0000i (ζ=0)	14.2179–0.0000i (ζ=0)	14.1930–0.0000i (ζ=0)
Pinned–pinned system				
First mode ω at u=2.00	7.5775+0.0000i (ζ=0)	7.5775+0.0050i (ζ=0.0007)	7.5775+0.0050i (ζ=0.0000)	7.5775+0.0051i (ζ=0.0007)
Second mode ω at u=2.00	37.4706+0.0000i (ζ=0)	37.4706+0.0050i (ζ=0.0001)	37.4706+0.0011i (ζ=0.0000)	37.4706+0.0061i (ζ=0.0002)
u_c	3.15 (1st mode buckling)	3.15 (1st mode buckling)	3.15 (1st mode buckling)	3.15 (1st mode buckling)
Clamped–clamped system				
First mode ω at u=2.00	21.1791+0.0000i (ζ=0)	21.1791+0.0050i (ζ=0.0002)	21.1791+0.0005i (ζ=0.0000)	21.1791+0.0055i (ζ=0.0003)
Second mode ω at u=2.00	60.1920+0.0000i (ζ=0)	60.1920+0.0050i (ζ=0.0001)	60.1920+0.0016i (ζ=0.0000)	60.1920+0.0066i (ζ=0.0001)
u_c	6.29 (1st mode buckling)	6.29 (1st mode buckling)	6.29 (1st mode buckling)	6.29 (1st mode buckling)

damping. At u=4.78, the second-mode locus crosses to the negative-Im(ω) half of the plane; as Im(ω_2)<0 and Re(ω_2)≠0, this indicates amplified oscillations or single degree-of-freedom flutter [11]. Moreover, the fourth-mode locus is observed to cross over to the negative-Im(ω) at $u \simeq 12.0$; thus, from the linear perspective, the system becomes unstable by single degree-of-freedom flutter in its fourth mode as well.

Table 2 summarizes the complex eigenfrequencies and damping factors at u=2.00, along with the calculated values of the critical flow velocities, u_c, for the thermoelastically damped beam. For comparison, the corresponding values are listed for beams with no damping ($\overline{\alpha} = 0,\ \mu = 0$ and $\sigma = 0$), viscous damping ($\overline{\alpha} = 0,\ \mu = 0$ and $\sigma = 0.01$), and a combination of viscous damping and TED ($\overline{\alpha} = 0,\ \mu = \mu_{\mathrm{TED}}$ and $\sigma = 0.01$).

5. Concluding remarks

Microscale pipes containing flow constitute an interesting new class of devices, both for enabling novel applications for MEMS, and for fundamental studies of the effects of size on fluid-structure interactions. This paper presented the first set of results on the effects of miniaturization on stability, damping, and frequency shifts in straight micromachined pipes containing an internal flow due to a single-phase incompressible fluid. The analysis was performed within the context of classical continuum mechanics, and numerical results were presented for the effects of size, boundary conditions, dissipation, materials, and flow velocity on the natural frequency, damping, and stability of flow-containing pipes. The results showed that: (i) flow-induced damping and frequency shifts in representative single-crystal silicon structures can exceed the typical specifications for resonant microsensors, and (ii) slender elastomeric pipes can become unstable by divergence and flutter at flow velocities of ~10 m/s. These results highlight the importance of considering fluid-structure interactions in the design of microscale resonators containing internal flow.

Acknowledgments

Financial support from the Natural Sciences and Engineering Research Council (NSERC) of Canada, the Canada Research Chairs program, and Fonds québécois de la recherche sur la nature et les technologies (FQRNT) are gratefully acknowledged.

References

[1] M. Li, H.X. Tang, M.L. Roukes, Ultra-sensitive NEMS-based cantilevers for sensing, scanned probe and very high-frequency applications, *Nature Nanotechnology* 2 (2007) 114–120.
[2] S. Prabhakar, M.P. Païdoussis, S. Vengallatore, Analysis of frequency shifts due to thermoelastic coupling in flexural-mode micromechanical and nanomechanical resonators, *Journal of Sound and Vibration* 323 (2009) 385–396.
[3] P. Enoksson, G. Stemme, E. Stemme, Fluid density sensor based on resonance vibration, *Sensors and Actuators A* 46 (1995) 327–331.
[4] P. Enoksson, G. Stemme, E. Stemme, A silicon resonant sensor structure for Coriolis mass-flow measurements, *Journal of Microelectromechanical Systems* 6 (1997) 119–125.
[5] D. Westberg, O. Paul, G.I. Andersson, H. Baltes, A CMOS-compatible device for fluid density measurements fabricated by sacrificial aluminum etching, *Sensors and Actuators A* 73 (1999) 243–251.
[6] T.P. Burg, M. Godin, S.M. Knudsen, W. Shen, G. Carlson, J.S. Foster, K. Babcock, S.R. Manalis, Weighing of biomolecules single cells and single nanoparticles in fluid, *Nature* 446 (2007) 1066–1069.
[7] M. Najmzadeh, S. Haasl, P. Enoksson, A silicon straight tube fluid density sensor, *Journal of Micromechanics and Microengineering* 17 (2007) 1657–1663.
[8] D. Sparks, R. Smith, V. Cruz, N. Tran, A. Chimbayo, D. Riley, N. Najafi, Dynamic and kinematic viscosity measurements with a resonating microtube, *Sensors and Actuators A* 149 (2009) 38–41.
[9] S. Deladi, J.W. Berenschot, N.R. Tas, G.J.M. Krijnen, J.H. de Boer, M.J. de Boer, M.C. Elwenspoek, Fabrication of micromachined fountain pen with in situ characterization possibility of nanoscale surface modification, *Journal of Micromechanics and Microengineering* 15 (2005) 528–534.
[10] K.-H. Kim, N. Moldovan, H.D. Espinosa, A nanofountain probe with sub-100 nm molecular writing resolution, *Small* 1 (2005) 632–635.
[11] M.P. Païdoussis, *Fluid Structure Interactions: Slender Structures and Axial Flow*, Vol. 1, Academic Press, London, 1998.
[12] M. Whitby, N. Quirke, Fluid flow in carbon nanotubes and nanopipes, *Nature Nanotechnology* 2 (2007) 87–94.
[13] J. Yoon, C.Q. Ru, A. Mioduchowski, Flow-induced flutter instability of cantilever carbon nanotubes, *International Journal of Solids and Structures* 43 (2006) 3337–3349.
[14] Y. Yan, X.Q. He, L.X. Zhang, Q. Wang, Flow-induced instability of double-walled carbon nanotubes based on an elastic shell model, *Journal of Applied Physics* 102 (2007) 044307.
[15] S.D. Senturia, *Microsystem Design*, Kluwer, Norwell, 2001.
[16] J.A. Pelesko, D.H. Bernstein, *Modeling MEMS and NEMS*, CRC Press, Boca Raton, 2002.
[17] H. Bruus, *Theoretical Microfluidics*, Oxford University Press, Oxford, UK, 2008.
[18] L.B. Freund, S. Suresh, *Thin Film Materials*, Cambridge University Press, Cambridge, UK, 2003.
[19] V.T. Srikar, S.M. Spearing, Materials selection in micromechanical design: an application of the Ashby approach, *Journal of Microelectromechanical Systems* 12 (2003) 3–10.
[20] V.T. Srikar, S.M. Spearing, A critical review of microscale mechanical testing methods used in the design of microelectromechanical systems, *Experimental Mechanics* 43 (2003) 238–247.
[21] K.P. Travis, B.D. Todd, D.J. Evans, Departure from Navier–Stokes hydrodynamics in confined liquids, *Physical Review E* 55 (1997) 4288–4295.
[22] J.-T. Cheng, N. Giordano, Fluid flow through nanometer-scale channels, *Physical Review E* 65 (2002) 031206.
[23] G. Chen, *Nanoscale Energy Transport and Conversion*, Oxford University Press, Oxford, UK, 2005.
[24] S. Groblacher, J.B. Hertzberg, M.R. Vanner, G.D. Cole, S. Gigan, K.C. Schwab, M. Aspelmeyer, Demonstration of an ultracold micro-optomechanical oscillator in a cryogenic cavity, *Nature Physics* 5 (2009) 485–488.
[25] M.P. Païdoussis, N.T. Issid, Dynamic stability of pipes conveying fluid, *Journal of Sound and Vibration* 33 (1974) 267–294.
[26] M.P. Païdoussis, P.E. Des Trois Maisons, Free vibration of a heavy damped vertical cantilever, *Journal of Applied Mechanics* 38 (1971) 524–526.

[27] T.B. Benjamin, Dynamics of a system of articulated pipes conveying fluids. II. Experiments, *Proceedings of the Royal Society (London) A* 261 (1961) 487–499.
[28] C. Mishra, Y. Peles, Cavitation in flow through a micro-orifice inside a silicon microchannel, *Physics of Fluids* 17 (2005) 013601.
[29] C. Zener, Internal friction in solids I: theory of internal friction in reeds, *Physical Review* 52 (1937) 230–235.
[30] R. Lifshitz, M.L. Roukes, Thermoelastic damping in micro- and nanomechanical systems, *Physical Review B* 61 (2000) 5600–5609.
[31] V.K. Kinra, K.B. Milligan, A second-law analysis of thermoelastic damping, *Journal of Applied Mechanics* 61 (1994) 71–76.
[32] S. Prabhakar, S. Vengallatore, Theory of thermoelastic damping in micromechanical resonators with two-dimensional heat conduction, *Journal of Microelectromechanical Systems* 17 (2008) 494–502.
[33] S. Prabhakar, S. Vengallatore, Thermoelastic damping in hollow and slotted microresonators, *Journal of Microelectromechanical Systems* 18 (2009) 725–735.